Energy Conversion and Management 93 (2015) 132–140

Contents lists available at ScienceDirect

Energy Conversion and Management

journal homepage: www.elsevier.com/locate/enconman

Co-pyrolysis behaviors of energy grass and lignite

Yanjun Guan, Ying Ma, Kai Zhang*, Honggang Chen, Gang Xu, Wenyi Liu, Yongping Yang

Beijing Key Laboratory of Emission Surveillance and Control for Thermal Power Generation, North China Electric Power University, Beijing 102206, China

ARTICLE INFO

Article history:
Received 22 October 2014
Accepted 3 January 2015

Keywords:
Energy grass
Lignite
Co-pyrolysis characteristics
Synergy
Kinetics

ABSTRACT

A kind of energy grass (giant reedgrass) with high calorific value, high production, low land requirement and low sulfur dioxide emission is introduced into lignite pyrolysis process in this paper. Individual pyrolysis and co-pyrolysis characteristics of energy grass and lignite are investigated by the thermogravimetric analyzer together with mass spectrometer. The individual decomposition indicates that energy grass possesses higher thermochemical reactivity and shorter devolatilization time than lignite. The maximum decomposition rate increases with increasing the heating rate for both energy grass and lignite. The mass spectrometric analysis reveals that the emission of sulfur dioxide from energy grass is much lower than that from lignite. The co-pyrolysis of energy grass and lignite blend is characterized by two-stage thermal degradation processes, which is dominant by energy grass content in the first stage but lignite in the second stage. No obvious interaction between energy grass and lignite is observed during the co-pyrolysis process under the operational conditions investigated in this study. Moreover, the distributed activation energy model is applied to determine the activation energy for the pyrolysis of energy grass, lignite and their blends.

© 2015 Elsevier Ltd. All rights reserved.

1. Introduction

Energy crops have gained extensive attention around the world. Compared with other biomass resources, energy crops can be grown on marginal land (sand, saline-alkali or industrial waste land) and used for phytoremediation of contaminated or poor soils. Many kinds of energy crops, such as willow, poplar, sweet sorghum, miscanthus, switchgrass, giant reedgrass and microalgae, have potential advantages for advanced biofuel feedstock. Compared to the retrofit in existing coal-based units, high investment costs are required for constructing a new plant to convert solely energy crops [1,2]. Therefore, the co-process with coal is a reasonable choice for utilizing energy crops at current stage.

The co-process of biomass and coal mainly includes pyrolysis, combustion and gasification. Pyrolysis process is considered not only as a promising technology to produce various chemicals and fuels, but also as a fundamental step in combustion or gasification of solid carbonaceous fuels [3–6]. As one of the most common techniques, thermogravimetric analysis (TGA) has been used to investigate the co-pyrolysis behaviors of biomass–coal blends in the past twenty years. Many results showed that the co-pyrolysis exhibited a simple additive effect of coal and different biomass, such as wood waste/wheat straw [1], pine chip [6,7], pine sawdust/sewage sludge [8], olive kernel/forest residue/cotton residue [9], olive kernel/straw [10], corncob [11], wood [12] and sawdust/switch grass [13]. On the other hand, several researchers [2,14,15] found the overall volatile yield of different blends exceeded the yield calculated from the additive behavior, by using hazelnut shell, sawdust, sugarcane bagasse, and corncob as biomass. However, Chen et al. [4] thought that the presence of microalgae could inhibit the thermal decomposition of biomass–coal blend. Clearly, a consensus on the effect of biomass had not yet reached during the co-pyrolysis processes of biomass–coal blends [2]. Furthermore, there are only a few investigations involving co-pyrolysis of energy crop and coal, such as by Chen et al. [4] and Masnadi et al. [13]. Therefore, it is necessary to fully understand the thermal behavior of energy grass–coal blend for designing and operating an efficient co-conversion unit.

The aim of this work is to explore the pyrolysis behaviors of energy crop (giant reedgrass) and lignite by using thermogravimetric analyzer together with mass spectrometer. The effects of heating rate and blending ratio are investigated in detail and the kinetic parameters of individual energy grass, lignite and their blends are obtained by the distributed activation energy model (DAEM).

---

* Corresponding author. Tel.: +86 10 61772413.
E-mail address: kzhang@ncepu.edu.cn (K. Zhang).

http://dx.doi.org/10.1016/j.enconman.2015.01.006
0196-8904/© 2015 Elsevier Ltd. All rights reserved.

2. Methods

2.1. Samples

The samples of lignite and energy grass (giant reedgrass) used in this study were collected from a farm in northern China. This kind of energy crop has following advantages: high calorific value (approximately 22.76 MJ/kg), high production (over fifteen years after planting as a perennial plant), and lower land requirement (growing rapidly in sandy, saline–alkali or industrial waste land). All samples were ground and sieved to the desired sizes less than 250 μm. To eliminate the effect of moisture content, the samples were dried in an oven set at 105 °C for 20 h. The blends of lignite and giant reedgrass were homogenized by vigorous mixing with desired mass percentages and subsequently rolling for 10 h. Generally, the chemical and physical properties of biomass are different from coal in terms of moisture, volatile matter, ash, density, calorific value, and porosity [14]. The proximate analysis and ultimate analysis summarized in Table 1 show that energy grass has higher volatile content, lower ash and fixed carbon contents than lignite. Moreover, the sulfur in energy grass is less than that in lignite.

2.2. Experiments

Pyrolysis characteristics of energy grass, lignite and their blends were determined by the thermogravimetric analyzer and mass spectrometer. Energy grass–lignite blends were prepared at the following mass ratios of 9:1, 8:2, 7:3, 6:4, 5:5, 4:6, 3:7, 2:8 and 1:9. Each sample was weighted 10 ± 0.2 mg and then loaded into an alumina crucible in nitrogen atmosphere under a fixed flow rate of 60 ml/min. The apparatus was purged with nitrogen for 30 min to ensure an inert environment before starting heating program. All experiments were conducted from the room temperature to 800 °C at a fixed heating rate of 5, 10, 15, 20 or 30 °C/min. The gaseous products released during pyrolysis process were examined by mass spectrometer coupled with thermogravimetric analyzer. The mass spectrometer was operated under a vacuum and detected the fragment ions intensity according to their respective mass to charge ratio (m/z). The ionizing voltage of electron impact ionization source was 70 eV, and the mass spectrum range was scanned from 0 to 150. Three repeated runs were conducted for each sample and the relative deviation was less than ±3%. Synergistic effect of energy grass and lignite was examined by comparing the mass loss versus temperature and char yield profiles.

3. Results and discussion

3.1. Individual pyrolysis of energy grass or lignite

3.1.1. Thermal decomposition characteristics

Taking the heating rate of 20 °C/min as an example, Fig. 1 shows the TG and DTG profiles of energy grass and lignite as a function of operational temperature. It can be evident that energy grass (around 68%) undergoes higher weight loss than lignite (around 41%) over the heating period, which is largely because the volatile matter in energy grass is higher than that in lignite as listed in Table 1. The DTG evolution profile indicates that the main thermal decomposition process of energy grass occurs in a temperature range of 150–500 °C. This is largely due to the decomposition characteristics of the thermally unstable hemicellulose (shoulder peak at 290 °C) and cellulose (highest peak at 347 °C), whilst lignin is decomposed over a broad temperature range without observable peak. As for lignite, the devolatilization occurs at a relatively low rate during almost the whole temperature range, which is quite different from energy grass. The main organic contents of lignite are decomposed in the temperature range of 300–600 °C, and the maximum pyrolysis rate of 2.63%/min occurs at 407 °C. The above phenomenon is due to the dense polycyclic aromatic hydrocarbons linked together by C=C bonds in lignite are more difficult to break than the polymers of hemicellulose, cellulose and lignin in biomass [16]. Moreover, a peak at 728 °C for lignite is assigned to the condensation of aromatic rings as the solid residue, which could only be coke at such high temperatures [17,18].

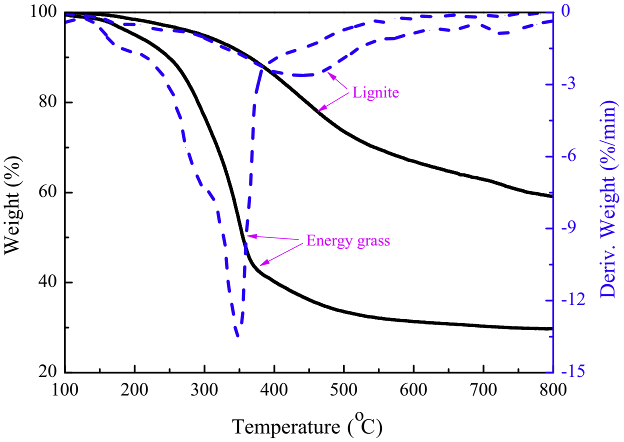

Fig. 1. TG and DTG profiles of energy grass and lignite.

3.1.2. Gaseous product emission characteristics

Gaseous thermal degradation products can provide more information related to the pyrolysis process. Fig. 2 displays the on-line mass spectrometric (MS) results of gaseous products with different m/z values. Hydrogen ($m/z = 2$) is detected mainly at higher temperature with peaks assigned at 650 °C for both the energy grass and lignite, as a result of charring process [17,18]. The ion CH_3^+ ($m/z = 15$) is formed from methane and the other organic compounds containing —CH_3 groups. The evolution profile exhibits two peaks between the temperatures of 400–550 °C for energy grass. The peak at lower temperature may arise from the compounds containing —CH_3 groups, whilst the peak at higher temperature is the methane [19]. As for lignite, CH_3^+ arises from methane is detected in the temperature range of 350–700 °C. The evolution of water ($m/z = 18$) below 200 °C is largely due to the releasing of free water and physically bonded water for both energy grass and lignite. Energy grass releases water between 250 °C and 400 °C due to the decomposition of hemicellulose and cellulose [19]. While lignite releases water between 250 °C and 600 °C due to the decomposition of chemically combined or chemically formed water [20]; and the main reason for water formation at higher

Table 1
Proximate analysis and ultimate analysis of energy grass and lignite.

	Proximate analysis (wt.%)				Ultimate analysis (wt.%)				
	Moisture	Vol	Ash	FC	C	H	O	N	S
Energy grass	7.25	61.55	16.30	14.90	38.91	5.50	38.03	2.24	0.40
Lignite	15.46	38.72	21.03	24.79	43.74	4.56	28.21	1.21	1.25

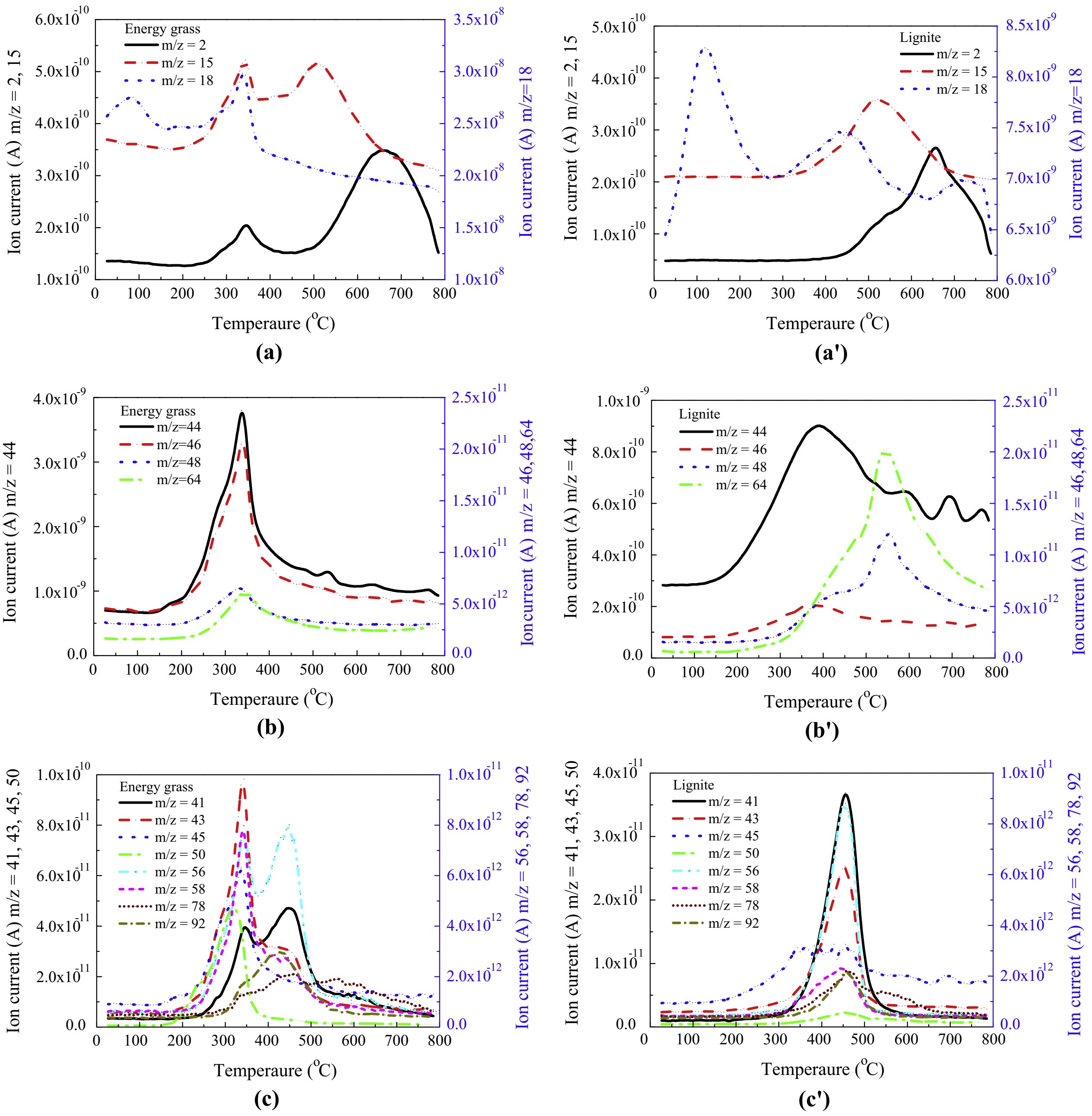

(a) (a')

(b) (b')

(c) (c')

Fig. 2. Evolution of the volatiles released during the pyrolysis.

temperature (over 600 °C) is the degradation of oxygen containing high molecular weight organic compounds by the catalytic effect of inorganic materials [21].

As observed in Fig. 2b and b′, carbon dioxide ($m/z = 44$) starts forming at 200 °C or so for both energy grass and lignite. The evolution of CO_2 increases sharply to a maximum at 337 °C and then decreases rapidly for energy grass, but decreases slowly after reaching a maximum at 389 °C for lignite. The lignite generates carbon dioxide by decomposing the aliphatic and aromatic carboxyl groups at low temperature [22], and the thermally more stable ether structure, quinines and oxygen-bearing heterocycles at high temperature [23]. Nitrogen dioxide ($m/z = 46$) is the main gaseous pollutant for energy grass pyrolysis, whose evolution is similar to carbon dioxide that exhibits a first-increase and then-decrease scenario at peak of 337 °C. Sulfur dioxide ($m/z = 48$, 64) is detected as the main gaseous pollutant for lignite, which starts from 200 °C or so and reaches maximums at 550 °C. Table 2 lists the releasing strength of carbon dioxide (CO_2), nitrogen dioxide (NO_2) and sulfur dioxide (SO_2) during pyrolysis by calculating the integrated area of each curve.

In addition, the other fragments with m/z values of 41, 43, 45, 50, 56, 58, 78 and 92 are also detected, as shown in Fig. 2c and c′. $m/z = 41$ consists of C_2HO^+ and $C_3H_5^+$, which are formed from

Table 2
Releasing strength of CO_2, NO_2 and SO_2 during pyrolysis.

	Integrate area/sample mass (E-10)		
	A_{CO_2}	A_{NO_2}	A_{SO_2}
Energy grass	502.06	2.23	1.27
Lignite	239.37	1.10	7.61

compounds containing —CH_2—CO— structure and unsaturated hydrocarbons, respectively [19]. $m/z = 43$ from propyl ($C_3H_7^+$), $m/z = 45$ from the fragment ion HCOO—, $m/z = 56$ from butane (C_4H_8), $m/z = 58$ from acetone (C_3H_6O), $m/z = 78$ and 92 from benzene and toluene, respectively [24]. It is clear that the organic components evolved slightly earlier and their formation rates are higher for energy grass.

In summary, the major degradation products of energy grass or lignite are hydrogen ($m/z = 2$), methane ($m/z = 15$), water ($m/z = 18$) and carbon dioxide ($m/z = 44$) based on the MS analysis.

3.1.3. Effect of heating rate

Similar evolution profiles of decomposition process are obtained at different heating rates of 5, 10, 15, 20 and 30 °C/min for both energy grass and lignite (Fig. 3). The increase in heating rate results in the peak temperature shifts to higher values, due to the higher heat transfer efficiency at lower heating rate. It was reported that the heating of biomass particles occurred more gradually and led better heat transfer to the inner portions of the particles at low heating rates [17,25,26]. Also the maximum rate of decomposition increases with increasing heating rate, which is because more thermal energy promotes better heat transfer between the surroundings and the inside of the sample [27,28]. Table 3 lists the yield of volatile matter from energy grass and lignite at different heating rates. The amount yield of volatiles increases with increasing the heating rate for both energy grass and lignite. The difference is that energy grass releases higher volatile matter than lignite under the same conditions.

Table 3
Volatile matter released at different heating rates.

Heating rate (°C/min)	5 (%)	10 (%)	15 (%)	20 (%)	30 (%)
Energy grass	60.36	67.41	66.11	70.09	77.19
Lignite	38.58	40.22	42.83	40.88	42.80

3.2. Co-pyrolysis of energy grass and lignite blends

3.2.1. Thermal decomposition characteristics

Fig. 4 displays the TG and DTG profiles of energy grass–lignite blends for various blending ratios at the heating rate of 20 °C/min. It is found that the co-pyrolysis process of energy grass–lignite blend could be characterized by two-stage thermal degradation, and the thermal decomposition is dominant by energy grass content in the first stage but lignite in the second stage. The weight loss and weight loss rate of the blends are between those of individual process. With an increase in blending ratio of energy grass to lignite, the weight loss and weight loss rate increase in the first stage but decrease in the second stage. This is consistent with the observations by Biagini et al. [8] and Aboyade et al. [29].

Several devolatilization characteristic parameters obtained at different heating rates and blending ratios are listed in Table 4. The tangent definition is adopted here: T_{in} is the initial decomposition temperature; T_f is the terminal decomposition temperature; DTG_{max} and T_{max} are the maximum degradation rate and the

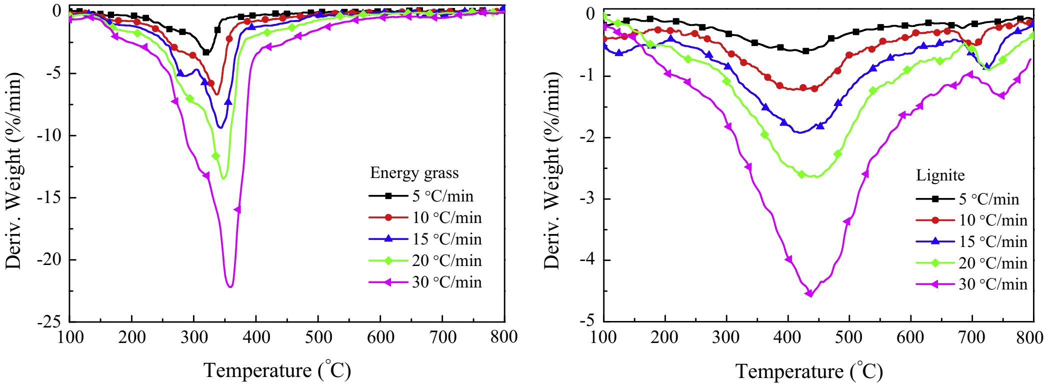

(a) Energy grass **(b) Lignite**

Fig. 3. DTG profiles of energy grass and lignite at different heating rates.

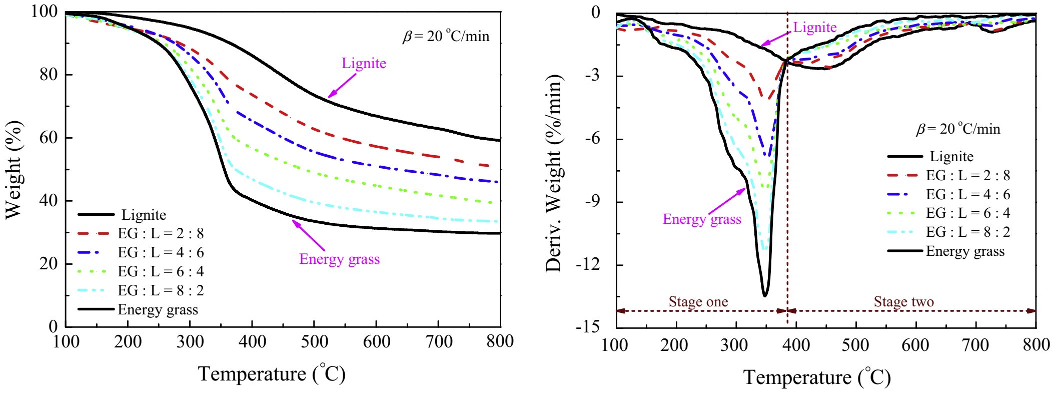

(a) TG profile **(b) DTG profile**

Fig. 4. Effect of blending ratio on the co-pyrolysis of energy grass and lignite.

Table 4
Characteristics parameters of co-pyrolysis process.

Sample	Heating rate (°C/min)	T_{in} (°C)	T_f (°C)	T_{max} (°C)	DTG_{max} (%/min)
EG:L (2:8)	5	260	436	322	1.95
	10	268	474	336	1.97
	15	275	490	343	2.93
	20	275	483	346	4.38
	30	284	475	358	7.23
EG:L (4:6)	5	257	376	324	2.02
	10	267	414	337	3.19
	15	269	411	343	5.04
	20	267	428	349	7.07
	30	273	435	354	12.03
EG:L (6:4)	5	263	374	317	2.22
	10	264	397	335	4.29
	15	280	392	342	7.08
	20	281	402	350	8.85
	30	284	413	357	14.96
EG:L (8:2)	5	260	364	321	2.70
	10	261	379	337	5.66
	15	263	390	346	8.35
	20	264	396	350	11.47
	30	271	409	360	17.86

Note: EG, energy crop; L, lignite.

corresponding temperature, respectively. It is clear that T_{in}, T_f, T_{max} and DTG_{max} shift to higher values with increasing the heating rate. The T_{in} and T_{max} are not sensitive with the blending ratio, and similar value ranges of T_{in} (260–285 °C) and T_{max} (320–360 °C) are obtained for different blends. This also implies that energy grass plays a dominant role in the first-stage pyrolysis process. An increase in energy grass–lignite blending ratio results in a higher maximum degradation rate. However, T_f increases with increasing the percent of lignite in the blends, which is also obtained by Vuthaluru [1] and Chen et al. [4].

3.2.2. Interaction between energy grass and lignite

In order to determine the "possible" interaction between energy grass and lignite during the co-pyrolysis process of their blends, the calculated and experimental weight losses at different heating rates and blending ratios are compared in Fig. 5. The calculated profiles were obtained assuming a simple additive behavior in weight loss between energy grass and lignite, as expressed below:

$$W_c = x_{EG}W_{EG} + x_L W_L \quad (1)$$

where W_c is the calculated weight loss of the blend, x_{EG} and x_L are the mass fraction of energy grass and lignite in the blend, respectively. W_{EG} and W_L are the weight loss of individual energy grass and lignite, respectively. Experimental and calculated curves match well with each other below 300 °C, whilst a slight deviation appears above 300 °C.

Moreover, the effect of blending ratio on char yield is presented in Fig. 6. In this study, the char yield is defined as the solid residue at 800 °C. The solid line is calculated by the weighted sum law of the averaged char yields of single fuel from different heating rates

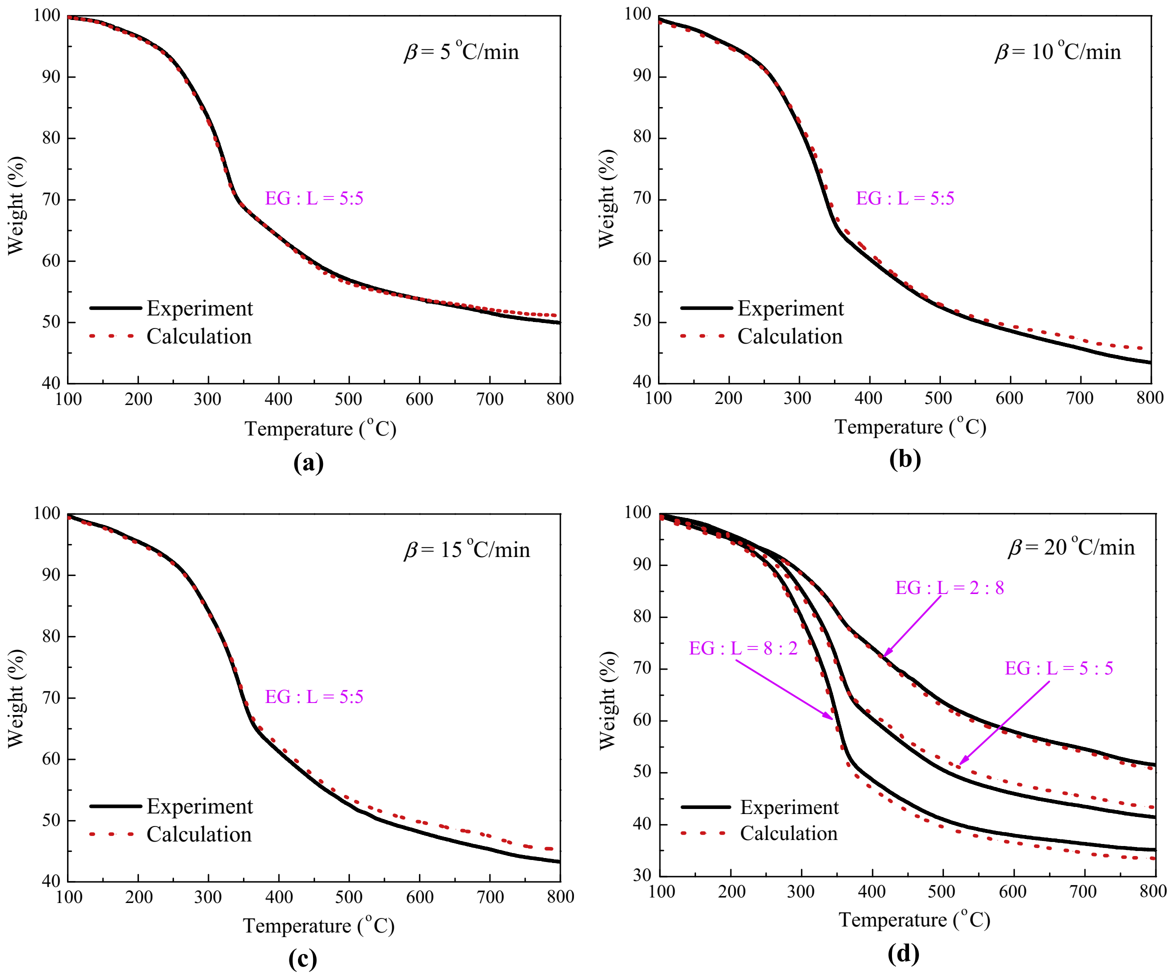

(a) (b) (c) (d)

Fig. 5. Comparison of experimental and calculated TG curves of energy grass–lignite blend.

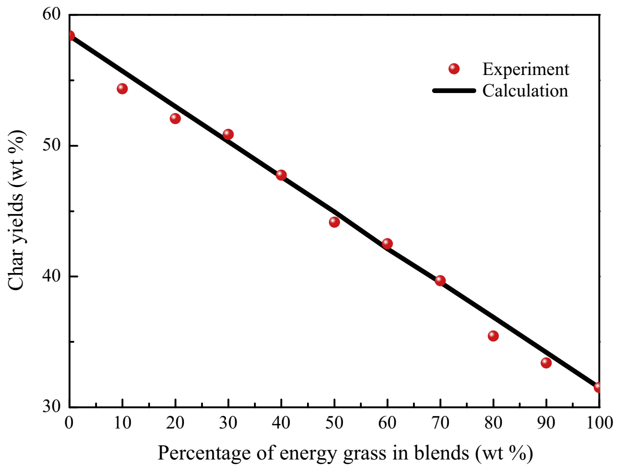

Fig. 6. Comparison of experimental and calculated char yields with different blending ratios.

of 5, 10, 15, 20 and 30 °C/min, and the experimental points are the average from different heating rates of 5, 10, 15, 20 and 30 °C/min. In Fig. 6, a corresponding decrease in the char yield is observed with increasing the mass fraction of energy grass in the blend, presenting an approximate liner relationship. This is due to the higher volatile and lower fixed carbon contents in energy grass than lignite. Experimental char yields against the blending ratio indicate the experimental values distribute in the vicinity of the calculated curve, and the maximum deviation from the theoretical value is 3.5% for blending ratio of 5:5. No significant difference between the experiment and the calculation assuming a simple additive behavior in char yields is obtained during the co-pyrolysis of energy grass and lignite. Similar results were obtained for different co-pyrolysis processes of coal and biomass, such as cotton residue, olive kernel, forest residue, rice husk, sugarcane bagasse, pine saw dust and oil palm [1,7,8,10,17,30].

According to the interaction examination between energy grass and lignite, the gaseous emissions should follow the similar additive behavior for different energy grass–lignite blends. This conclusion is also supported by the MS analysis as expected. Hydrogen ($m/z = 2$), methane ($m/z = 15$), water ($m/z = 18$), carbon dioxide ($m/z = 44$), nitrogen dioxide ($m/z = 46$), sulfur dioxide ($m/z = 48$, 64) and organic fragments, as detected during the individual pyrolysis process, are recorded over the co-pyrolysis process. The gaseous products emission peaks of blends are found in agreement with the combination of single fuel.

3.3. Activation energy of pyrolysis

The weight loss of sample with increasing temperature is constantly measured and recorded using thermogravimetric analyzer, and the kinetics can be determined by the Arrhenius equation [31]. Many different reaction models are used in coal/biomass pyrolysis

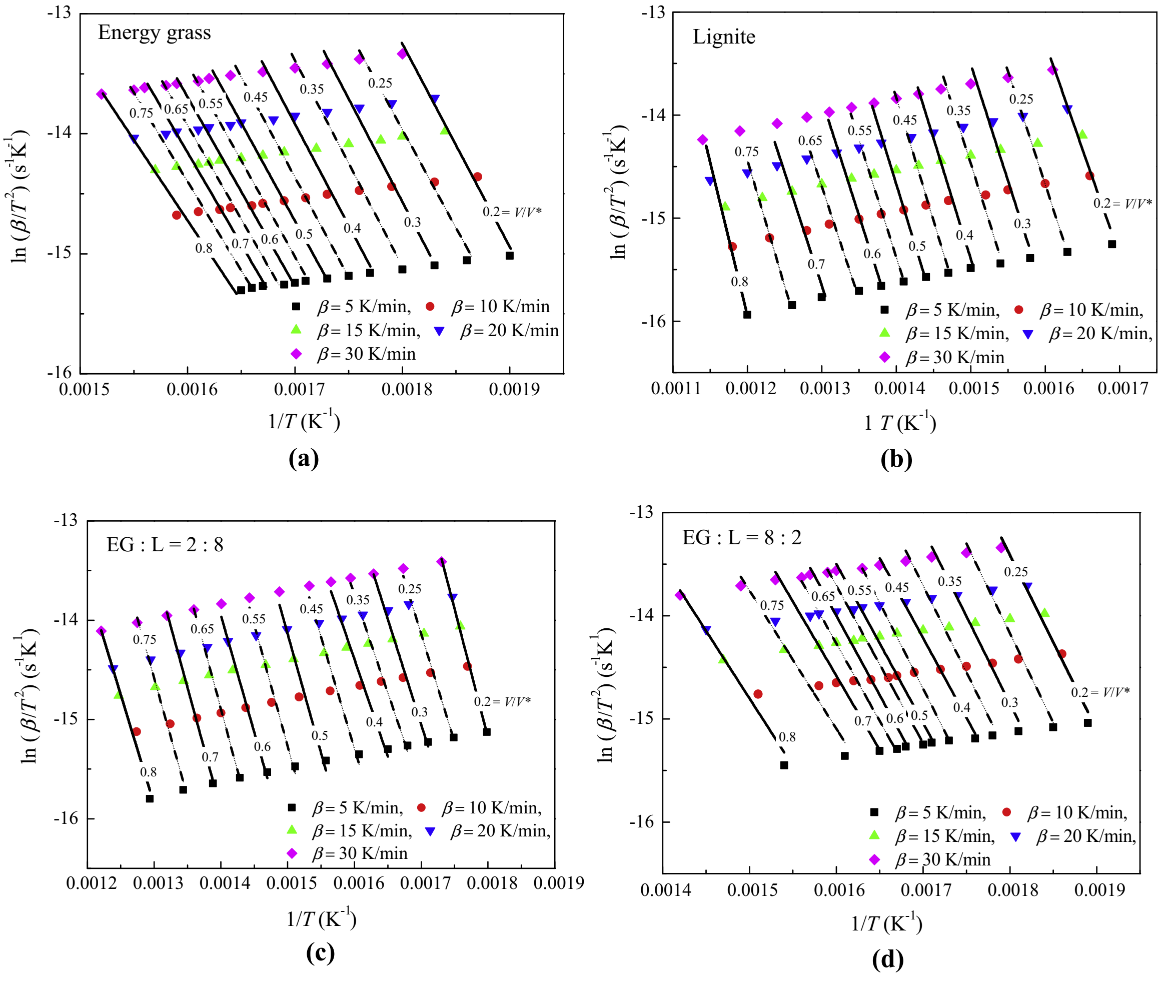

Fig. 7. Arrhenius plots of ln (β/T^2) vs. $1/T$ for energy grass and lignite.

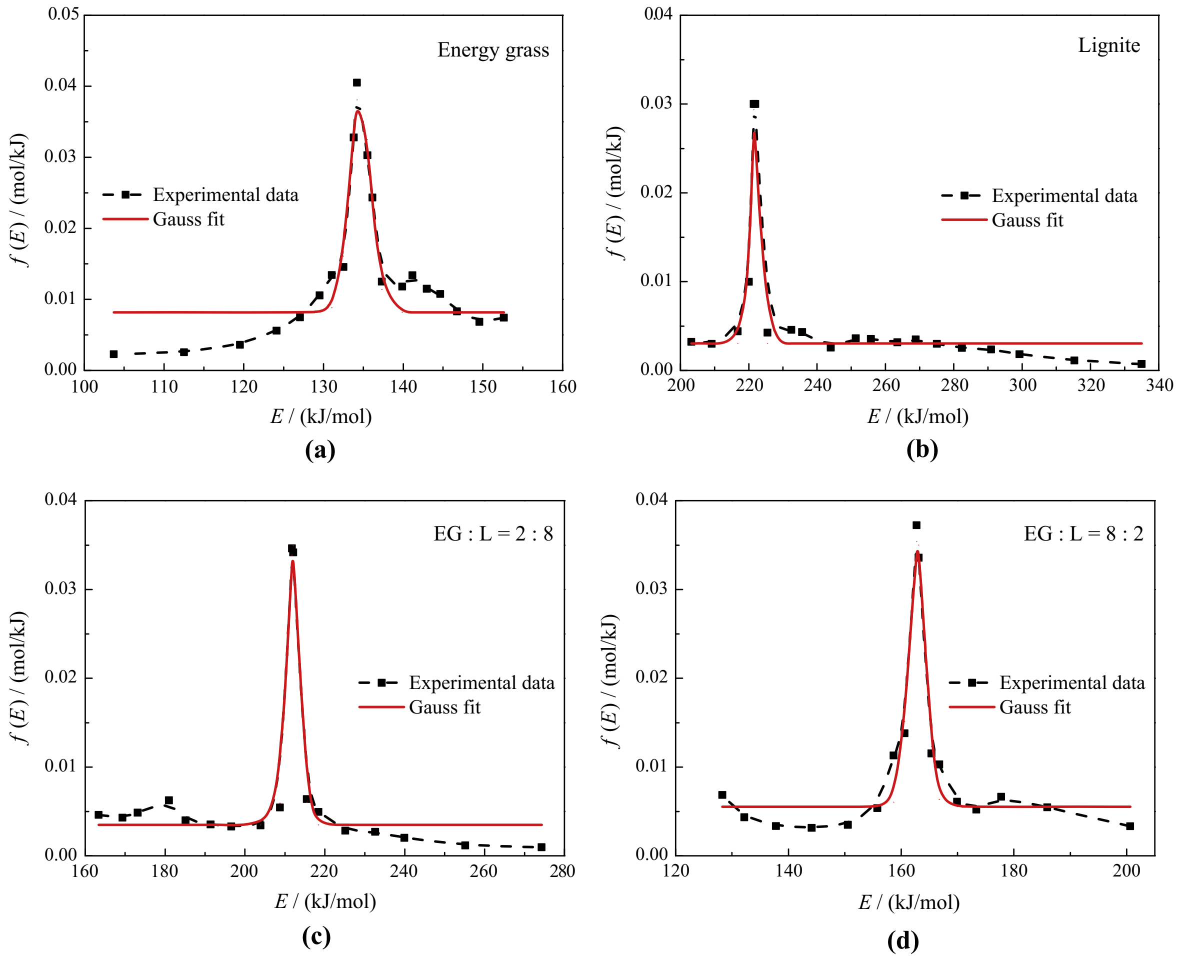

Fig. 8. Distributions of $f(E)$ during pyrolysis process.

process [8,12,17,32,33]. Among these models, the distributed activation energy model (DAEM) was considered to be one of the most important methods to reflect the real complexity of coal, coke and other carbonized solid fuels [34]. The activation energy corresponding to the conversion rate is not directly related to the heating rate by DAEM, which can give an objective description of the pyrolysis process. Currently, the DAEM has been employed successfully in analyzing the complex reactions involved in the co-pyrolysis process of biomass–coal blends [28,35,36]. This model assumes an infinite number of irreversible first-order parallel reactions with different activation energies, and the difference in activation energies is represented by a distribution function. The model is expressed as:

$$1-\frac{V}{V^*}=\int_0^\infty \exp\left(-k_0\int_0^t \mathrm{e}^{-E/RT}\mathrm{d}t\right)f(E)\mathrm{d}E \tag{2}$$

where V is the weight loss by time t, V^* is the total weight loss at the end of pyrolysis, k_0 is the frequency factor corresponding to E, and $f(E)$ is the distribution function of activation energy, representing the variation of the activation energies of those first-order irreversible reactions. The distribution function value plays an important role in determining the contribution rate of the total volatiles released [36]. Eq. (2) is often simplified to the expression as [37,38]:

$$1-\frac{V}{V^*}=\int_0^\infty \Phi(E,T)f(E)\mathrm{d}E \tag{3}$$

According to Eqs. (2) and (3), Eq. (4) should be expressed as:

$$\Phi(E,T)=\exp\left(-\frac{k_0}{\beta}\int_0^t \mathrm{e}^{-E/RT}\mathrm{d}t\right) \tag{4}$$

A step function U at an activation energy E_s for $\Phi(E,T)$ is postulated to give an approximation for Eq. (4) as [37]

$$\Phi(E,T)=U(E-E_s) \tag{5}$$

and thus Eq. (3) is simplified to

$$1-\frac{V}{V^*}=\int_{E_s}^\infty f(E)\mathrm{d}E \tag{6}$$

This condition is found to hold approximately when $\Phi(E,T)\cong 0.58$ for many combinations of k_0 and $f(E)$ from the examinations by Miura and Maki [38] and Shen et al. [39]. As a result, the Arrhenius equation can be described as follows:

$$\ln\left(\frac{\beta}{T^2}\right)=\ln\frac{k_0R}{E}+0.6075-\frac{E}{R}\frac{1}{T} \tag{7}$$

By Eq (7), both E and k_0 can be obtained from the linear relationship between $\ln(\beta/T^2)$ and $(1/T)$ at selected V/V^* value. The procedure for estimating the $f(E)$ and k_0 can be summarized as follows [38]:

(1) To measure V/V^* vs. T relationships at least three different heating rates.
(2) To calculate the values of $\ln(\beta/T^2)$ and $(1/T)$ at the same V/V^* for different heating rates.

(3) To plot $\ln(\beta/T^2)$ vs. $(1/T)$ at the same V/V^* values, and determine E and k_0 from the slopes and intercepts, respectively.
(4) To plot V/V^* vs. E and differentiate the curve to obtain $f(E)$.

As typical examples, Arrhenius plots of different fuels in Fig. 7 display linear and parallel development. The correlation coefficients are all above 0.95, which means the thermal degradation processes of energy grass, lignite and their blends can be described by a set of single reactions. According to the DAEM, the distributions of activation energy (E) values are obtained from the slopes of the liner-fitting lines, and each conversion rate has individual corresponding activation energy during the thermal decomposition process. Since the low correlation is observed for conversion below 0.2 or above 0.8, the above cases are left out of the calculations to avoid introducing an incorrect interpretation of the phenomena [40].

Fig. 8 shows the activation energy (E) distributions for energy grass, lignite and their blends. The $f(E)$ curves of different fuels display Gaussian distributions as the previous investigations [36,38]. The peak E value of energy grass is 134 kJ/mol and has a corresponding $f(E)$ of 0.038 mol/kJ. However, the activation energy values of lignite are higher than energy grass. A peak E value of 221 kJ/mol and a corresponding $f(E)$ of 0.029 mol/kJ are respectively observed for the lignite, which is consist with the study of Miura and Maki [38]. For the energy grass–lignite blends, the values of E are distributed between those of the single fuels. With increasing percent of energy grass in the blend, the activation energy distribution shifts to energy grass. This also implies that the DAEM is able to predict the pyrolysis behavior of the energy grass–lignite blends.

4. Conclusions

Thermal behaviors and kinetics of energy grass, lignite and their blends are investigated based on thermogravimetric analysis together with mass spectrometry. The following conclusions are obtained from this work:

(1) Energy grass undergoes higher weight loss in a narrow temperature range, whilst lignite is decomposed at a relatively low rate over the whole temperature range. The maximum decomposition rate increases with increasing the heating rate for both energy grass and lignite.
(2) The mass spectrometric analysis indicates that the hydrogen, methane, water and carbon dioxide are the major degradation products for either energy grass or lignite. The emission of sulfur dioxide from energy grass is much lower than that from lignite during the pyrolysis process.
(3) The co-pyrolysis process of energy grass–lignite blends is characterized by two-stage thermal degradation. Energy grass plays a dominant role in the first stage, and lignite in the second stage.
(4) The co-pyrolysis of energy grass and lignite reveals additive properties under the experimental conditions investigated. The thermal decomposition and gaseous product emission characteristics of blends are close to the combination of the single fuels.
(5) The distributed activation energy model (DAEM) gives an objective description of the pyrolysis process of single fuel or energy grass–lignite blend. The activation energy of energy grass is smaller than that of lignite. With increasing the percent of energy grass in the blend, the activation energy distribution of energy grass–lignite blend shifts to energy grass.

Acknowledgements

Financial support from the National Key Technology R&D Program of China (2012BAC24B01), National Natural Science Foundation of China (91434120), Fundamental Research Funds for the Central Universities (2014ZD06), and the 111 Project (B12034) is gratefully acknowledged.

References

[1] Vuthaluru H. Thermal behaviour of coal/biomass blends during co-pyrolysis. Fuel Process Technol 2003;85:141–55.
[2] Aboyade A, Görgens J, Carrier M, Meyer E, Knoetze J. Thermogravimetric study of the pyrolysis characteristics and kinetics of coal blends with corn and sugarcane residues. Fuel Process Technol 2013;106:310–20.
[3] Biagini E, Fantei A, Tognotti L. Effect of the heating rate on the devolatilization of biomass residues. Thermochim Acta 2008;472:55–63.
[4] Chen C, Ma X, He Y. Co-pyrolysis characteristics of microalgae Chlorella vulgaris and coal through TGA. Bioresour Technol 2012;117:264–73.
[5] Zheng A, Zhao Z, Chang S, Huang Z, He F, Li H. Effect of torrefaction temperature on product distribution from two-staged pyrolysis of biomass. Energy Fuels 2012;5:2968–74.
[6] Pan Y, Velo E, Puigjaner L. Pyrolysis of blends of biomass with poor coals. Fuel 1996;75:412–8.
[7] Jones J, Kubacki M, Kubica K, Ross A, Williams A. Devolatilisation characteristics of coal and biomass blends. J Anal Appl Pyrolysis 2005;74:502–11.
[8] Biagini E, Lippi F, Petarca L, Tognotti L. Devolatilization rate of biomasses and coal–biomass blends: an experimental investigation. Fuel 2002;81:1041–50.
[9] Kastanaki E, Vamvuka D, Grammelis P, Kakaras E. Thermogravimetric studies of the behavior of lignite–biomass blends during devolatilization. Fuel Process Technol 2002;77–78:159–66.
[10] Vamvuka D, Pasadakis N, Kastanaki E, Grammelis P, Kakaras E. Kinetic modeling of coal/agricultural by-product blends. Energy Fuels 2003;17:549–58.
[11] Sonobe T, Worasuwannarak N, Pipatmanomai S. Synergies in co-pyrolysis of Thai lignite and corncob. Fuel Process Technol 2008;9:1371–8.
[12] Lu K, Lee W, Chen W, Lin T. Thermogravimetric analysis and kinetics of co-pyrolysis of raw/torrefied wood and coal blends. Appl Energ 2013;105:57–65.
[13] Masnadi MS, Habibi R, Kopyscinski J, Hill JM, Bi X, Lim CJ, et al. Fuel characterization and co-pyrolysis kinetics of biomass and fossil fuels. Fuel 2014;117 Part B:1204–14.
[14] Haykiri-Acma H, Yaman S. Synergy in devolatilization characteristics of lignite and hazelnut shell during co-pyrolysis. Fuel 2007;86:373–80.
[15] Park D, Kim S, Lee S, Lee J. Co-pyrolysis characteristics of sawdust and coal blend in TGA and a fixed bed reactor. Bioresour Technol 2010;101:6151–6.
[16] Yılgın M, Deveci Duranay N, Pehlivan D. Co-pyrolysis of lignite and sugar beet pulp. Energy Convers Manage 2010;51:1060–4.
[17] Idris S, Rahman N, Ismail K, Alias A, Rashid Z, Aris M. Investigation on thermochemical behaviour of low rank Malaysian coal, oil palm biomass and their blends during pyrolysis via thermogravimetric analysis (TGA). Bioresour Technol 2010;101:4584–92.
[18] Shi L, Liu Q, Guo X, Wu W, Liu Z. Pyrolysis behavior and bonding information of coal – A TGA study. Fuel Process Technol 2013;108:125–32.
[19] Várhegyi G, Czégény Z, Jakab E, McAdam K, Liu C. Tobacco pyrolysis. Kinetic evaluation of thermogravimetric–mass spectrometric experiments. J Anal Appl Pyrolysis 2009;86:310–22.
[20] Li X, Matuschek G, Herrera M, Wang H, Kettrup A. A study on combustion of Chinese coals by TA/MS. J Anal Appl Pyrolysis 2003;67:393–406.
[21] Karayildirim T, Yanik J, Yuksel M, Bockhorn H. Characterisation of products from pyrolysis of waste sludges. Fuel 2006;85:1498–508.
[22] Asadieraghi M, Wan Daud WMA. Characterization of lignocellulosic biomass thermal degradation and physiochemical structure: effects of demineralization by diverse acid solutions. Energy Convers Manage 2014;82:71–82.
[23] Arenillas A, Pevida C, Rubiera F, García R, Pis J. Characterisation of model compounds and a synthetic coal by TG/MS/FTIR to represent the pyrolysis behaviour of coal. J Anal Appl Pyrolysis 2004;71:747–63.
[24] Yani S, Zhang D. Transformation of organic and inorganic sulphur in a lignite during pyrolysis: influence of inherent and added inorganic matter. P Combust Inst 2009;32:2083–9.
[25] Biagini E, Barontini F, Tognotti L. Devolatilization of biomass fuels and biomass components studied by TG/FTIR technique. Ind Eng Chem Res 2006;45:4486–93.
[26] Ceylan S, Topçu Y. Pyrolysis kinetics of hazelnut husk using thermogravimetric analysis. Bioresour Technol 2014;156:182–8.
[27] Kim S, Park D, Kim S. Pyrolytic characteristics of Jatropha seedshell cake in thermobalance and fluidized bed reactors. Korean J Chem Eng 2013;30:1162–70.
[28] Li L, Zhao N, Fu X, Shao M, Qin S. Thermogravimetric and kinetic analysis of Spirulina wastes under nitrogen and air atmospheres. Bioresour Technol 2013;140:152–7.

[29] Aboyade A, Carrier M, Meyer E, Knoetze J, Görgens J. Model fitting kinetic analysis and characterisation of the devolatilization of coal blends with corn and sugarcane residues. Thermochim Acta 2012;530:95–106.

[30] Ismail K, Zakaria Z, Ishak MAM. Thermal behaviour study of Mukah Balingian coal and rice husk blends during pyrolysis via thermogravimetric analysis. In: Paper Presented at the Brunei International Conference on Engineering and Technology, BICET 2005, Brunei.

[31] Kılıç M, Pütün AE, Uzun BB, Pütün E. Converting of oil shale and biomass into liquid hydrocarbons via pyrolysis. Energy Convers Manage 2014;78:461–7.

[32] Ko KH, Rawal A, Sahajwalla V. Analysis of thermal degradation kinetics and carbon structure changes of co-pyrolysis between macadamia nut shell and PET using thermogravimetric analysis and 13C solid state nuclear magnetic resonance. Energy Convers Manage 2014;86:154–64.

[33] Çepelioğullar Ö, Pütün AE. Thermal and kinetic behaviors of biomass and plastic wastes in co-pyrolysis. Energy Convers Manage 2013;75:263–70.

[34] Várhegyi G. Aims and methods in non-isothermal reaction kinetics. J Anal Appl Pyrolysis 2007;1–2:278–88.

[35] Wang G, Li W, Li B, Chen H. TG study on pyrolysis of biomass and its three components under syngas. Fuel 2008;87:552–8.

[36] Li C, Suzuki K. Kinetic analyses of biomass tar pyrolysis using the distributed activation energy model by TG/DTA technique. J Therm Anal Calorim 2009;98:261–6.

[37] Miura K. A new and simple method to estimate $f(E)$ and $k_0(E)$ in the distributed activation energy model from three sets of experimental data. Energy Fuels 1995;9:302–7.

[38] Miura K, Maki T. A simple method for estimating $f(E)$ and $k_0(E)$ in the distributed activation energy model. Energy Fuels 1998;12:864–9.

[39] Shen D, Gu S, Jin B, Fang M. Thermal degradation mechanisms of wood under inert and oxidative environments using DAEM methods. Bioresour Technol 2011;102:2047–52.

[40] Damartzis T, Vamvuka D, Sfakiotakis S, Zabaniotou A. Thermal degradation studies and kinetic modeling of cardoon (*Cynara cardunculus*) pyrolysis using thermogravimetric analysis (TGA). Bioresour Technol 2011;102:6230–8.